journal of the mechanical behavior of biomedical materials 110 (2020) 103858

Contents lists available at ScienceDirect

Journal of the Mechanical Behavior of Biomedical Materials

journal homepage: http://www.elsevier.com/locate/jmbbm

3D full-field strain in bone-implant and bone-tooth constructs and their morphological influential factors

Yuxiao Zhou [a], Chujie Gong [b], Mehran Hossaini-Zadeh [c], Jing Du [a,*]

[a] Department of Mechanical Engineering, Pennsylvania State University, University Park, PA, 16802, United States
[b] Department of Biomedical Engineering, Pennsylvania State University, University Park, PA, 16802, United States
[c] Department of Oral Maxillofacial Pathology, Medicine and Surgery, Temple University, Philadelphia, PA, 19140, United States

ARTICLE INFO

Keywords:
Dental implant
Strain
Micro-CT
Digital volume correlation

ABSTRACT

The biomechanics of bone-tooth and bone-implant interfaces affects the outcomes of several dental treatments, such as implant placement, because bone, tooth and periodontal ligament are living tissues that adapt to the changes in mechanical stimulations. In this work, mechanical testing coupled with micro-CT was performed on human cadaveric mandibular bone-tooth and bone-implant constructs. Using digital volume correlation, the 3D full-field strain in bone under implant loading and tooth loading was measured. Concurrently, bone morphology and bone-implant and bone-tooth contact were also measured through the analysis of micro-CT images. The results show that strain in bone increased when a tooth was replaced by a dental implant. Strain concentration was observed in peri-implant bone, as well as in the buccal bone plate, which is also the clinically-observed bone resorption area after implant placement. Decreasing implant stability measurements (resonance frequency analysis and torque test) indicated increased peri-implant strain, but their relationships may not be linear. Peri-implant bone strain linearly increased with decreasing bone-implant contact (BIC) ratio. It also linearly decreased with increasing bone-tooth/bone-implant contact ratio. The high strain in the buccal bone plate linearly increased with decreasing buccal bone plate thickness. The results of this study revealed 3D full-field strain in bone-tooth and bone-implant constructs, as well as their several morphological influential factors.

1. Introduction

Bone is a living tissue and adapts to the changes in mechanical loads (Cowin and Hegedus, 1976; Frost, 1994; Roberts et al., 2004; Verner et al., 2016; Wolff, 1986; Yang et al., 2017). Therefore, the biomechanics of bone-tooth and bone-implant constructs affects the outcomes of several dental treatments, such as prosthodontic (Kratochvil and Caputo, 1974), orthodontic (Nanda, 2005), and dental implant treatments (Brunski, 1992). There is a need to study and compare the biomechanics of bone-tooth and bone-implant constructs and their influential factors.

Bone has a complex hierarchical structure and is inhomogeneous, anisotropic, and viscoelastic (Rho et al., 1998). Dentin in tooth has also been shown to be viscoelastic (Zhang et al., 2014). The periodontal ligament (PDL) supports the teeth in their sockets and allows them to withstand the mastication forces. It consists cells and an extracellular compartment, which mainly is collagen fiber bundles in ground substance (Nanci and Bosshardt, 2006). The PDL has non-linear load-displacement relationship (Yoshida et al., 2001) and viscoelastic material properties (Dorow et al., 2002).

Micro X-ray computed tomography (micro-CT) has often been used to assess changes in bone morphology, microstructure, and bone density due to disease, treatment, diet, and other factors (de Bakker et al., 2017; Hammond et al., 2018; Oestreich et al., 2015; Perosky et al., 2016; Scheller et al., 2016). Micro-CT and synchrotron micro-CT have also been used to study the fracture and toughening of bone and changes in them due to age, disease, and treatment (Busse et al., 2013; Launey et al., 2010; Lloyd et al., 2017; Oestreich et al., 2015; Ritchie et al., 2009; Zimmermann et al., 2011; Zimmermann and Ritchie, 2015). Mechanical testing coupled with micro-CT and digital volume correlation have been applied to map strain in trabecular bone blocks (Bay et al., 1999; Gillard et al., 2014; Jiroušek et al., 2011; Liu and Morgan, 2007), cortical bone (Christen et al., 2012; Dall'Ara et al., 2014), whole bones (Hussein et al., 2012; Kusins et al., 2019; Tozzi et al., 2016), bone-cement interfaces (Tozzi et al., 2012; Zhu et al., 2016). This method has been extended to map strain in bone-implant constructs first in our prior work and later

* Corresponding author. 316B Leonhard Building, Penn State University, University Park, PA, 16802, United States.
E-mail addresses: yyz5239@psu.edu (Y. Zhou), gongchujie@gmail.com (C. Gong), mhossaini@temple.edu (M. Hossaini-Zadeh), jingdu@psu.edu (J. Du).

https://doi.org/10.1016/j.jmbbm.2020.103858
Received 17 March 2020; Received in revised form 8 May 2020; Accepted 10 May 2020
Available online 19 May 2020
1751-6161/© 2020 Elsevier Ltd. All rights reserved.

also in other studies (Du et al., 2015; Le Cann et al., 2017; Zhou et al., 2019).

In this study, mechanical testing coupled with micro-CT was performed on cadaveric mandible bone-implant and bone-tooth constructs. Using digital volume correlation of micro-CT images under no-load and loaded conditions, the 3D full-field strain in bone under implant loading and tooth loading were measured and compared. Concurrently, bone morphology and bone-implant and bone-tooth contact were also measured through the analysis of micro-CT images. Statistical analysis was carried out to study the possible influential factors for strain in bone and to study the relationship between clinical implant stability measurements and the strain in bone. The implications of the results were discussed as related to the buccal bone resorption after dental implant treatments.

2. Material and methods

2.1. Specimen preparation

This study was exempted by Institutional Review Board (IRB) at Pennsylvania State University (STUDY00007794) on 7/27/2017. Three fresh frozen cadaveric mandibles were obtained from National Disease Research Interchange (NDRI). 7 single-rooted teeth were chosen as test sites, including central incisors, lateral incisors, canines, and premolars. The sample preparation protocol was similar to those used in our prior work (Du et al., 2015). The mandibles were thawed and sectioned by a diamond saw (Isomet 1000 Precision Cutter, Buehler, Lake Bluff, IL) to specimens that each contained a tooth to be tested and its two adjacent teeth. The sectioned specimens were then partly embedded in polymethylmethacrylate (PMMA, Ortho-Jet BCA, Lang Dental, Wheeling, IL). The crowns of the teeth to be tested were slightly polished with sandpaper (CarbiMet Plain 320, Buehler, Lake Bluff, IL) to create a flat surface for better load transfer in the subsequent mechanical testing on teeth (section 2.2). The top one-third of the crowns for the two adjacent teeth were cut off to avoid load transfer during mechanical test (section 2.2).

Following the mechanical testing on teeth (section 2.2), the tested teeth were extracted and dental implants (SLActive® Roxolid®, TiZr, Straumann, Basel, Switzerland) were installed using a dental surgical drill kit (Straumann BL, stainless steel, Straumann, Basel, Switzerland) by a practicing dentist. This type of implant was chosen because it has been commonly used in clinical settings (French et al., 2015) and it was also used in our prior proof-of-concept work (Du et al., 2015). One implant was placed in each specimen, except for the one bone-tooth specimen that fractured during tooth exaction. The implant specifications were chosen and the implant installation was performed according to the manufacturer's instruction and clinical standards by the practicing dentist. Peak insertion torque value (ITV) was measured by torque gauges (ATG6CN-S and BTG60CN-S, Tohnichi, Tokyo, Japan) during implant placement. Implant stability quotient (ISQ) was measured by an implant stability meter (Osstell ISQ, Osstell AB, Gothenburg, Sweden). Conical healing abutments (Straumann, Basel, Switzerland) were then installed onto implants.

2.2. Mechanical testing coupled with micro-CT

Mechanical testing was performed on the bone-tooth and bone-implant specimens, respectively, using a loading device (CT5000, Deben, Suffolk, UK) coupled with micro-CT (Phoenix v|tome|x L300, GE, Boston, MA). The specimens were kept moist during testing. The loading protocol was similar to that used in our prior work (Du et al., 2015). A compressive load was applied onto the single tooth or the implant at the center of each specimen at a constant displacement rate of 0.1 mm/min until the load reached 100 N, because the forces measured during mastication and swallowing were reported to be between 5 and 364 N (Kelly, 1999). Then the load was held at 100 N for 1 h, when we observed the change of specimen height was minimal, which indicated that the viscous components in the specimens were settled and clear micro-CT images could be obtained. Micro-CT scans were performed before loading and after 1-hr holding, respectively, using a voltage of 150 kV, a current of 100 μA for bone-teeth specimens and a voltage of 180 kV, a current of 85 μA for bone-implant specimens. Micro-CT images with isometric voxel size of 15 μm were obtained.

2.3. Bone morphology analysis

The micro-CT images (Fig. 1) were converted from 32-bit to 8-bit without resampling in ImageJ (National Institute of Health, Maryland, USA) and then cropped and segmented using the watershed algorithm in Avizo (FEI Visualization Sciences Group, Burlington, MA). The teeth, implant and alveolar bone were labeled, respectively. Using the segmented images, the bone-tooth contact area, $A_{b\text{-}t}$, and bone-implant contact area, $A_{b\text{-}i}$, and total implant area, A_i were calculated, respectively. The bone-implant contact (BIC) ratio, $A_{b\text{-}i}/A_i$ and bone-tooth/bone-implant contact area ratio, $A_{b\text{-}t}/A_{b\text{-}i}$, were calculated, respectively. The thickness of the buccal (lip-side) bone plate, t_b, was measured on the transverse section of micro-CT images of teeth where the buccal bone plate was the thinnest (Fig. 2a). The thickness was considered unchanged after implant placement.

2.4. Bone strain analysis

3D full-field displacement field inside the alveolar bone under tooth loading and implant loading was calculated using digital volume correlation (DVC) of micro-CT images of alveolar bone at no-load and loaded conditions in DaVis software (LaVision, Goettingen, Germany). Besides the alveolar bone, other objects in the images were masked and only the correlation windows that contain more than 50% valid voxels were used in the following correlation. Multiple passes of correlation were carried out with reducing correlation window size of $512 \times 512 \times 512$, $256 \times 256 \times 256$ and $128 \times 128 \times 128$ voxels. The overlap ratio between adjacent correlation windows was 50%. Fast Fourier transformation (FFT) was used for the first step and Direct Correlation (DC) was used in subsequent steps. Strain components were computed using a centered finite difference (CFD) scheme. A few displacement vectors with correlation value below 0.8 or peak ratio below 1.5 were removed from the results and replaced by an interpolation of neighboring vectors.

3D full-field strain field inside alveolar bone was obtained by taking numerical differentiation of the displacement field. The partial derivatives were mostly approximated by central difference, except for the correlation windows at the boundaries, where forward or backward difference was used. The strain in about 10 correlation windows in the middle of the buccal bone was extracted and defined as mid-buccal bone strain for bone-tooth and bone-implant specimens, respectively. Also, for bone-implant specimens, a sub-volume covering the implant surface with a thickness of 0.75 mm was defined as the peri-implant region. Its shape was similar to a cylindrical hollow tube with one end capped. The strain in it was extracted and defined as peri-implant bone strain.

The accuracies of the results were estimated using the following three methods. First, the micro-CT images at loaded condition were restored based on the calculated displacement vectors. They were then compared with the micro-CT images at no-load condition visually to ensure the accuracy of the calculated displacement vectors. Second, the noise level in the results was evaluated using a zero-strain approach (Bay et al., 1999; Hardisty and Whyne, 2009; Verhulp et al., 2004; Zauel et al., 2006) on two sets of images both taken at no-load condition. Third, the uncertainties in the results were also estimated by the constant-strain analyses using repeated images virtually deformed by 1% in the vertical direction, which was also the loading direction (Comini et al., 2019).

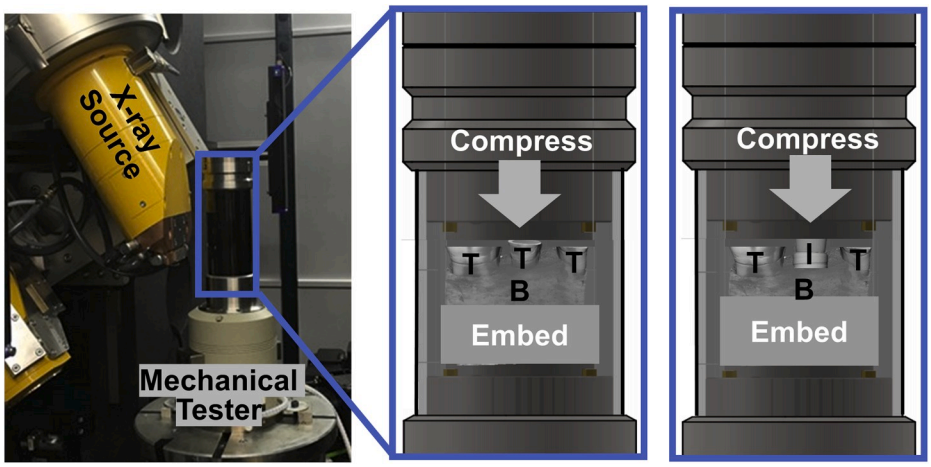

Fig. 1. Schematics of experimental setup and sample preparation. T – tooth; I – Implant; B – Bone.

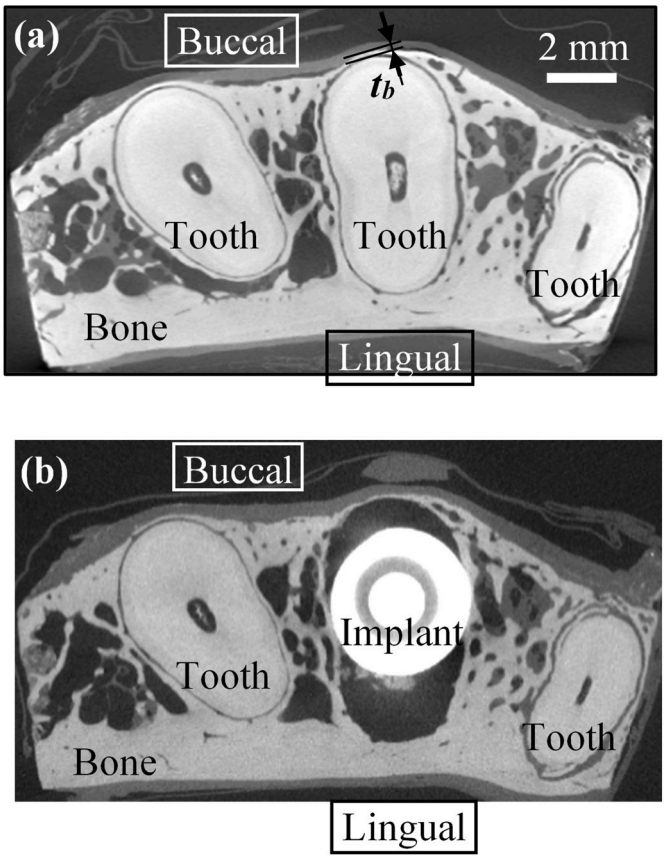

Fig. 2. A transverse slice of micro-CT images shows a bone-tooth specimen and the definition of buccal bone plate thickness, t_b. Specimen in (a) went through tooth extraction and implant placement and became a bone-implant specimen in (b).

2.5. Statistical analysis

Statistical analysis was carried out using Minitab software (Minitab, LLC, State College, PA). The maximum principal strain in every correlation window inside bone was summarized in box plots for each specimen, including the mean and median values. The term strain in the following statistical analysis refers to the maximum principal strain. Analysis of variance (ANOVA) was carried out for the mean values of strain, using a mixed-effects model with each bone specimen as a random effect and tooth/implant as a fixed effect. The bone-tooth specimen that fractured during tooth extraction was excluded in the ANOVA. For bone-implant specimens, simple linear regression was performed between ISQ and ITV. Simple linear regression was also performed between ISQ and peri-implant strain, between ITV and peri-implant strain, as well as between $A_{b\text{-}t}/A_{b\text{-}I}$ and peri-implant strain. Simple linear regression was also performed between the mid-buccal bone strain and the buccal bone plate thickness, t_b, for bone-tooth and bone-implant specimens, respectively.

3. Results

3.1. Strain distribution in bone

The typical 3D field of maximum principal strain in one bone specimen before and after implant placement was compared in Fig. 3a. Before implant placement, the strain was relatively uniformly distributed in alveolar bone around the tooth, and was below 0.28% in most part of the specimen, except some strain concentration regions in the buccal bone plate, where the strain was 0.40% to 0.50%. After implant placement, more regions in bone exhibited strain concentration, including some regions in contact with implant, bone crest, and buccal/lingual bone plate, where strain could sometimes be above 0.8%.

Fig. 3b summarizes the maximum principal strain in all correlation windows for all bone specimens before and after implant installation. The strain in bone ranged from −0.15% to 1.27% under tooth loading. The buccal bone plate of specimen 7 was very thin and fractured during tooth extraction, hence no implant was installed in it. The strain in bone ranged from −0.13% to 0.94% under implant loading. The median values of strain ranged from 0.08% to 0.18% in bone under tooth loading and ranged from 0.15% to 0.40% for bone under implant loading. In each bone specimen, the median value of strain increased after implant placement. The ANOVA results show that the mean strain values were significantly different ($P < 0.05$) in the bone-tooth category and the bone-implant category. The difference between individual bone specimens is not statistically significant ($P > 0.05$).

The accuracies of the results were estimated by the zero-strain approach and constant-strain analysis. The zero-strain approach resulted in a strain of 0.0106% ± 0.0290%. The constant-strain analyses using 1% virtually deformed images resulted in 0.969% ± 0.151% for bone-tooth and 0.949% ± 0.116% for bone-implant specimen.

3.2. ITV, ISQ and peri-implant strain

For all implants, the ITV was measured to be between 2.5 and 54 cN m, and the ISQ was measured to be between 7 and 60. The average

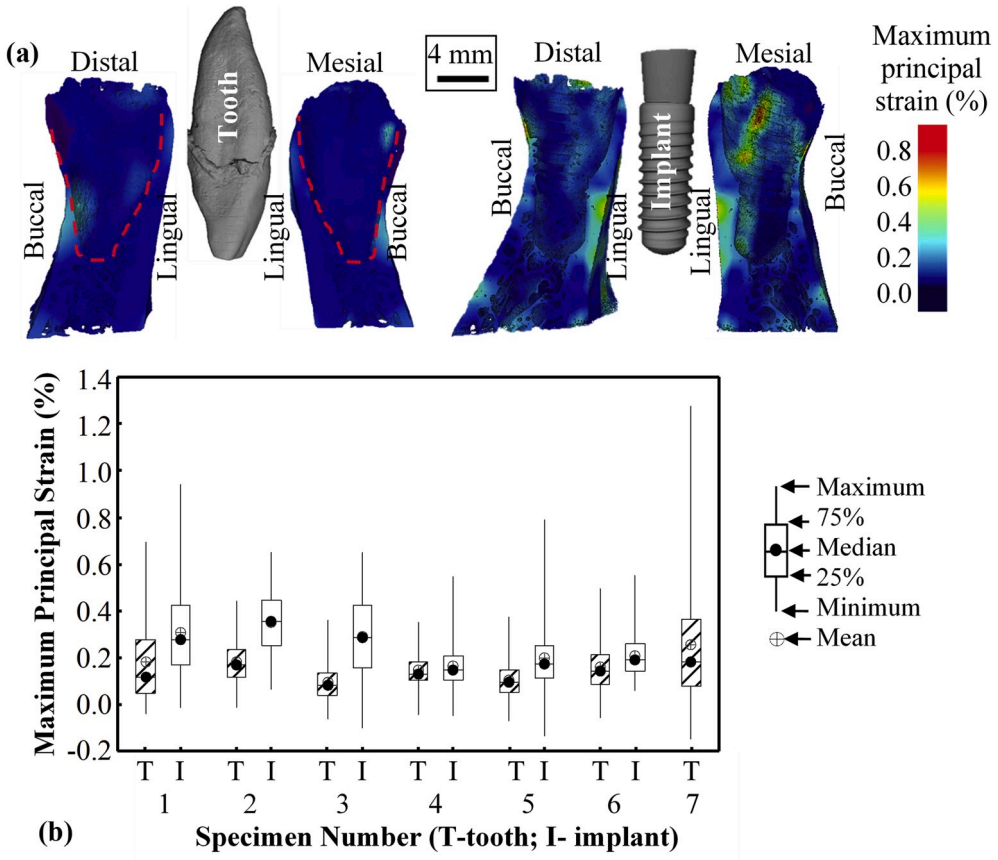

Fig. 3. (a) Experimentally measured typical strain distribution inside the same piece of bone under tooth loading and under implant loading. The 3D rendered images were virtually sectioned and rotated to reveal the strain inside the two halves of bone. (b) Measured maximum principal strain inside bone under tooth loading and implant loading for all specimens.

maximum principal strain in peri-implant region was measured to be between 0.17% and 0.26%. Generally, ISQ increased with increasing ITV; peri-implant strain decreased with increasing ISQ; and, it also decreased with increasing ITV. Simple linear regression between ISQ and ITV resulted in a coefficient of determination, R^2, of 94.5% and the p-value P = 0.001 (Fig. 4a), between ISQ and the peri-implant strain resulted in R^2 of 65.8% and the P = 0.05, between ITV and peri-implant strain resulted in R^2 of 63.8% and the P = 0.057.

3.3. Contact area and peri-implant strain

In bone-tooth specimens, teeth were in full contact with alveolar bone via periodontal ligament (PDL) (Fig. 5a), and the bone-tooth contact area, $A_{b\text{-}t}$, was measured to be from 93.83 to 240.61 mm^2. After implant placement, dental implant was only in partial contact with the alveolar socket, usually in the distal and mesial sides, while the buccal and lingual sides were not in contact with bone (Figs. 2a and 5b). The bone-implant contact area, $A_{b\text{-}i}$, was measured to be from 15.64 to 109.82 mm^2. The BIC ratio was calculated to be from 7.00% to 53.64%, and the bone-tooth/bone-implant contact ratio was calculated to be from 0.85 to 12.83.

The average maximum principal strain in peri-implant region decreased with increasing BIC ratio. Linear regression analysis between peri-implant strain and BIC ratio resulted in R^2 of 87.1% and $P < 0.01$ (Fig. 6a). Peri-implant strain increased with the increasing bone-tooth/bone-implant contact ratio. Also, the results of simple linear regression between them show that R^2 is 91.9% and $P < 0.01$ (Fig. 6b).

3.4. Buccal bone plate thickness of and strain

The thickness of the buccal bone plate was measured to be from 0.10 to 0.18 mm for all specimens. The average maximum principal strain in the buccal bone plate was measured to be from 0.13% to 0.95% under tooth loading, and 0.28%–0.84% under implant loading. It reduces with increasing buccal bone plate thickness, for bone-tooth specimens and bone-implant specimens, respectively (Fig. 7). Simple linear regression between the strain in buccal bone and the thickness of buccal bone resulted in R^2 of 77.2% and $P < 0.05$ for bone-tooth specimens and R^2 of 82.9% and $P < 0.01$ for bone-implant specimens.

4. Discussion

4.1. Implant stability and strain in bone

Implant stability is a prerequisite for implant osseointegration and long-term positive outcomes for osseointegrated implants (Javed and Romanos, 2010; Lioubavina-Hack et al., 2006). Clinical methods to measure implant stability include percussion test, torque test (insertion torque and reverse torque), periotest, and resonance frequency analysis. The results of this study show that there was a strong linear relationship between the results of torque test (ITV) and resonance frequency analysis (ISQ) (Fig. 4a), which is consistent with the prior discoveries by some other research groups (Akça et al., 2006; Gallardo et al., 2016; Jun et al., 2010; Turkyilmaz et al., 2009). But it should also be noted that some studies showed that the correlation between torque value and ISQ was not statistically significant (Akça et al., 2007; Akkocaoglu et al., 2005).

The fundamental reasons behind the correlation between implant

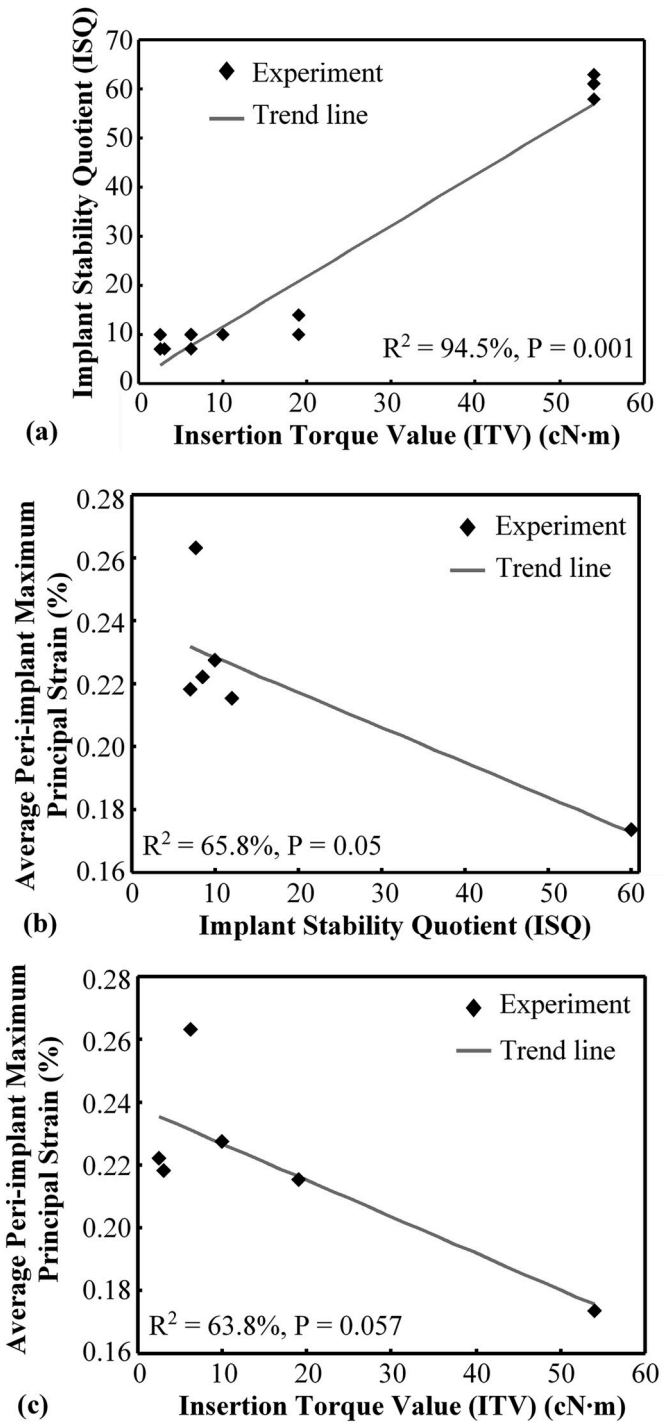

Fig. 4. (a) Simple linear regression between ITV and ISQ (R^2 = 94.5%, P = 0.001); (b) Simple linear regression between ISQ and average maximum principle strain in peri-implant region (R^2 = 65.8%, P = 0.05); (c) Simple linear regression between ITV and peri-implant strain (R^2 = 63.8%, P = 0.057).

stability and implant success are associated with the mechanobiology of bone-implant interface. Under loading, implant micromotion causes stress and strain field in bone, which then affects the cellular responses (Leucht et al., 2007) and contributes to bone-implant interface healing (Wazen et al., 2013) or damage (Cha et al., 2015). Measurement of strain in bone is therefore important in the study of implant biomechanics and implant success. However, conventional strain measurement methods, such as strain gauges (Howell and Manly, 1948), photoelasticity (Kratochvil and Caputo, 1974), Moiré fringe pattern (Wang and Weiner, 1998), electronic speckle pattern interferometry (Zhang et al., 2001) and digital image correlation (Chuang et al., 2008), can only measure strain on the surface of bone, teeth or dental materials. The experimental methods used in this study, mechanical testing coupled with micro-CT and digital volume correlation, are advantageous over the conventional methods, because the 3D internal strain in bone and the 3D internal structure of bone-implant constructs can be measured concurrently.

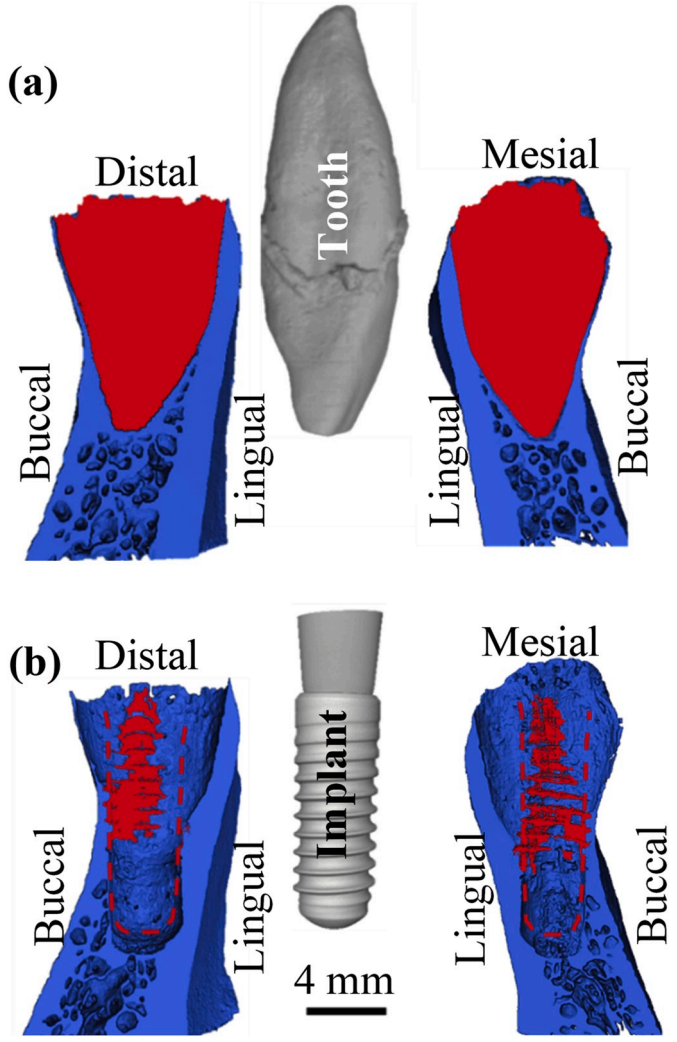

Fig. 5. Typical (a) bone-tooth contact area, $A_{b\text{-}t}$ and (b) bone-implant contact area, $A_{b\text{-}i}$ are highlighted in red for the same piece of bone before and after implant placement. The 3D rendered images were virtually sectioned and rotated to reveal the contact area.

4.2. *Influential factors of strain in bone*

The results of this study show that when the teeth were extracted and replaced by implants, the increment of mean strain in bone is statistically significant ($P < 0.05$) (Fig. 3). It can be attributed to the fact that the interfacial area for load transmission usually decreased after implant placement (Fig. 5). The results also reveal two strain concentration regions, the bone-implant contact region and the buccal bone plate, which are consistent with our prior findings through experimental measurements (Du et al., 2015) and numerical simulations (Mao et al., 2019). Moreover, the influential factors for these two strain concentration regions were investigated in this study, respectively.

Under loading, the implants pressed on the alveolar bone and caused high strain concentration at bone-implant contact regions. The results of

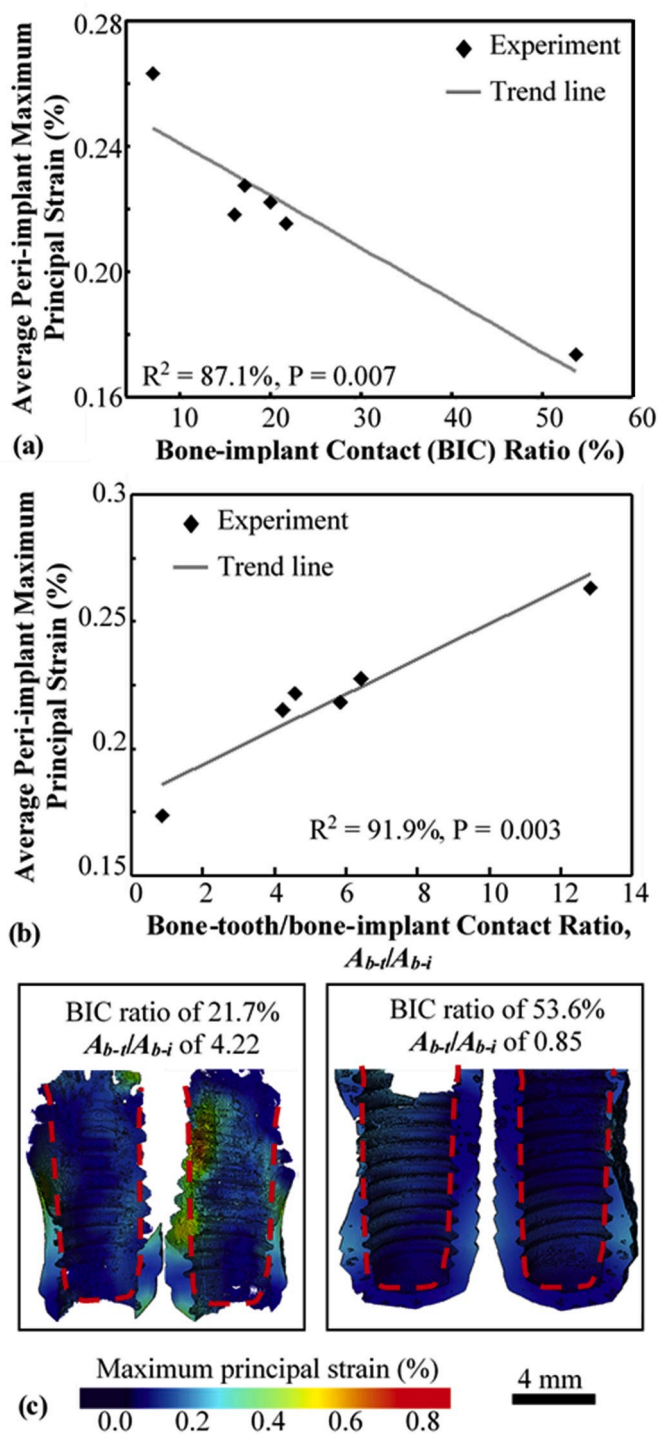

Fig. 6. (a) Simple linear regression between the peri-implant strain and BIC ratio ($R^2 = 87.1\%$, $P < 0.01$). (b) Simple linear regression between peri-implant strain and bone-tooth/bone-implant contact ratio ($R^2 = 91.9\%$, $P < 0.01$). (c) Comparison of experimentally measured strain distribution in the peri-implant region for two implant-bone specimens with different contact areas. The 3D rendered images were virtually sectioned to reveal the strain inside bone.

this study show that the peri-implant strain linearly decreased with increasing BIC ratio (Fig. 6a). It is consistent with the discoveries by Hsu et al. (2013), who found that strain on the surface of bone-mimicking polymeric foams increased when BIC ratio decreased. In other implant studies, BIC ratio was commonly used to represent the degree of osseointegration after implant treatment (Proff et al., 2008; Veis et al., 2007).

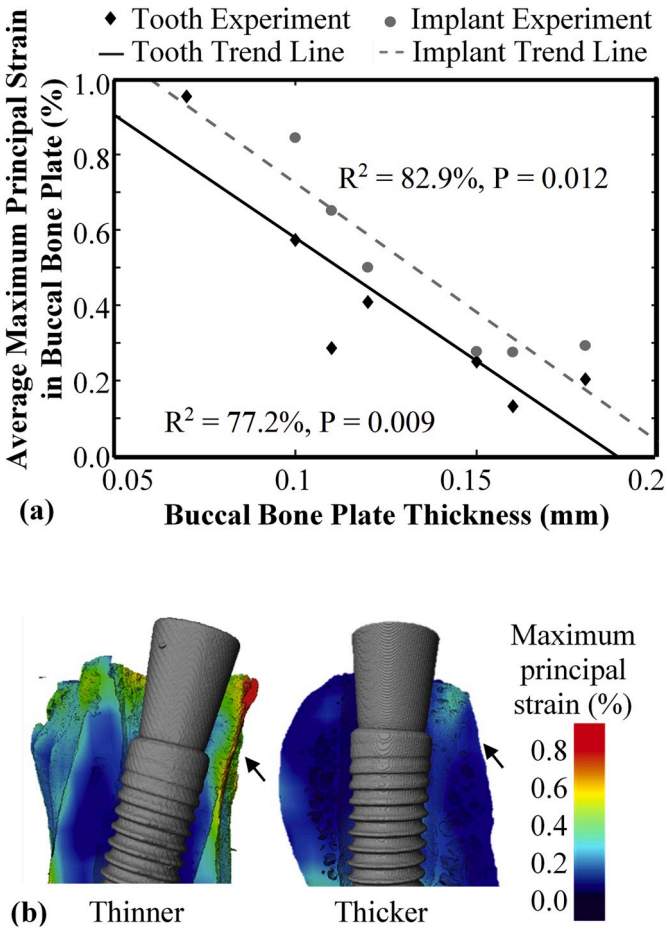

Fig. 7. (a) Simple linear regression between the buccal bone plate thickness and the average maximum principal strain in mid-buccal bone plate under tooth loading ($R^2 = 77.2\%$, $P < 0.05$) and implant loading ($R^2 = 82.9\%$, $P < 0.05$). (b) Comparison of experimentally measured strain distribution in two implant-bone specimens with buccal bone plate of different thicknesses (0.1 mm and 0.15 mm). The 3D rendered images were virtually sectioned to reveal the strain inside bone.

The results of this study also show that the linear relationship between peri-implant strain and the ratio between bone-implant and bone-tooth contact area was statistically significant (Fig. 6b), which has never been reported before to the best of our knowledge. Chewing and biting forces on teeth were transmitted to bone through bone-tooth interfaces, whereas those on implants were transmitted to bone through bone-implant interfaces (Fig. 5). Assuming those forces were similar before and after implant placement, if the strain in alveolar bone surrounding teeth were similar under normal physiological condition, the strain in peri-implant bone should be inversely proportional to the bone-implant/bone-tooth contact ratio, i.e. proportional to the bone-tooth/bone-implant contact ratio, which is consistent with the discoveries in this study (Fig. 6b).

Moreover, the relationships between the stability measurement (ISQ and ITV) and peri-implant strain (Fig. 4b and c) suggested that although the peri-implant strain generally decreased with increasing ISQ and ITV, the linear correlations were not statistically significant ($P \geq 0.05$). The strain-ISQ and strain-ITV relationships might not be linear. The literature also shows that the relationships between implant stability measurements and BIC ratio are still inconclusive. In some studies, the BIC ratio was shown to be significantly correlated with ISQ (Huang et al., 2013; Park et al., 2011) and ITV (Hsu et al., 2013; Liu et al., 2012). While other studies showed no statistically significant correlation between BIC ratio and ISQ (Abrahamsson et al., 2009; Jun et al., 2010;

Manresa et al., 2014; Scarano et al., 2006) or between BIC ratio and ITV (Degidi et al., 2009). Although ISQ and ITV are current clinical standards for implant stability measurements, they may not be linearly correlated with BIC contact or peri-implant strain. It is needed to further investigation their relationship with larger specimen size or more complex models.

Upon tooth/implant loading, strain concentration also appeared in the buccal bone plate. The results of this study show that thinner buccal bone plate resulted in higher strain in buccal bone plate for bone-tooth constructs (Fig. 7a). Implant placement and implant loading further increased the strain in buccal bone plate, compared with that in bone-tooth constructs (Fig. 7a). Thinner buccal bone plate resulted in higher strain for bone-implant constructs as well (Fig. 7a). The high strain in buccal bone can be attributed to the fact that it is thinner and less stiff than the lingual bone (Fig. 2). Using finite element simulation, Li et al. also found that the stress and strain for buccal bone increased with decreasing bone thickness, and the initial bone thickness subsequently affected the mechanobiology and bone resorption (Yoda et al., 2017). A commonly seen clinical and esthetic complication of dental implants is associated with the mid-buccal bone loss and its reason is poorly understood (Chen and Buser, 2014, 2009). Upon further investigations, the mechanobiology altered by abnormal strain in thin buccal bone plate may provide a possible explanation for the mid-buccal bone loss.

Besides the maximum principal strain, median and minimum principal strain, and effective strain were also calculated. No statistically significant correlation was found between these strain components and stability measurements (ISQ and ITV). No statistically significant correlation was found between these strain components and influential factors being studied in this paper (BIC ratio, bone-tooth/bone-implant contact ratio, and buccal plate thickness).

4.3. Limitations of this study

In this study, besides the strain inside bone, the strain at the surface of bone, at the bone-tooth interface, and bone-implant interface was also reported. To deal with these interfaces, only the images of bone were used in the correlation calculation, and the images of other objects were masked. Also, only the correlation windows that contained more than 50% valid voxels were used in the correlation calculation. But, the results at these interfaces may still be less accurate than those inside the bone.

There are multiple factors affecting implant mechanics and implant stability that were not studied in this work. These factors include bone density and quality, implant shape, design and surface characteristics, and surgical technique. A suggested direction of future work would be individual-specific numerical models with controlled influential factors. It should also be noted that the sample size in this study was small. Another limitation of this study is that simplified loading condition was used in this study whereas the physiological loading conditions are more complex. Hence, other loading conditions are considered as possible directions for future work.

Moreover, the experimental setup in this study was related to the immediate placement and immediate loading in the clinical setting, since cadaveric specimens had no biological activities (Du et al., 2015). A possible direction of future work would be *in vivo* studies, in which the bone strain during and after osseointegration can be investigated. Bone substitutes were not used in this study, but they were sometimes used to fill the space between the implant and the socket in the clinical environment (Schlegel and Donath, 1998). It is worth studying the effects of these bone substitute materials, such as Bio-Oss, on the bone-implant contact and on the strain in bone in future works.

5. Conclusions

This paper presents the results of an experimental study on the bone-tooth and bone-implant biomechanics. Using mechanical testing coupled with micro-CT, the bone morphology, internal contact interfaces, and the 3D full-field strain in bone were measured. Several influential factors for the strain in bone were also studied. Overall, strain in mandibular bone increased when a tooth was replaced by a dental implant. Two strain concentration regions in bone-implant constructs were revealed to be the peri-implant region and the buccal bone plate. Decreasing implant stability measurements (ISQ and ITV) indicates increased peri-implant strain, but their relationships may not be linear. Peri-implant bone strain linearly increased with decreasing BIC ratio or increasing bone-tooth/bone-implant contact ratio. The high strain in the buccal bone plate in bone-tooth constructs further increased when the teeth were replaced by implants. Also, it linearly increased with decreasing buccal bone plate thickness, for both bone-tooth and bone-implant constructs. The results of this study paved the way for future work including *in vivo* investigation on the evolution of bone morphology, bone-implant interface, and bone strain after implant placement.

Author contribution

Yuxiao Zhou: Conceptualization, Methodology, Formal analysis, Investigation, Software, Writing - Original Draft, Visualization. Chujie Gong: Software. Mehran Hossaini-Zadeh: Investigation, Resources, Writing - Review & Editing. Jing Du: Conceptualization, Writing - Review & Editing, Supervision, Project administration, Funding acquisition.

Declaration of competing interest

The authors declare that they have no known competing financial interests or personal relationships that could have appeared to influence the work reported in this paper.

CRediT authorship contribution statement

Yuxiao Zhou: Conceptualization, Methodology, Formal analysis, Investigation, Software, Writing - original draft, Visualization. **Chujie Gong:** Software. **Mehran Hossaini-Zadeh:** Investigation, Resources, Writing - review & editing. **Jing Du:** Conceptualization, Writing - review & editing, Supervision, Project administration, Funding acquisition.

Acknowledgment

This work was supported by the National Center for Advancing Translational Sciences, National Institutes of Health [Grant UL1TR002014, 2017]. The content is solely the responsibility of the authors and does not necessarily represent the official views of the NIH. The support was made available through Penn State Clinical and Translational Science Institute (CTSI). The authors are grateful to Dr. Timothy Ryan and Mr. Timothy Stecko at the Center for Quantitative Imaging (CQI) at Penn State University for technical support on micro-CT scans. The authors would also like to extend the gratitude to Dr. Mosuk Chow and Dr. Prabhani Kuruppumullage Don for the consultation statistical analysis, and Mr. Richard Prevost and Mr. Aditya Gupta from LaVision Inc. for consultation regarding DaVis software.

References

Abrahamsson, I., Linder, E., Lang, N.P., 2009. Implant stability in relation to osseointegration: an experimental study in the Labrador dog. Clin. Oral Implants Res. 20, 313–318. https://doi.org/10.1111/j.1600-0501.2008.01646.x.

Akça, K., Akkocaoglu, M., Cömert, A., Tekdemir, I., Cehreli, M.C., 2007. Bone strains around immediately loaded implants supporting mandibular overdentures in human cadavers. Int. J. Oral Maxillofac. Implants 22, 101–109.

Akça, K., Chang, T., Tekdemir, I., Fanuscu, M.I., 2006. Biomechanical aspects of initial intraosseous stability and implant design: a quantitative micro-morphometric

analysis. Clin. Oral Implants Res. 17, 465–472. https://doi.org/10.1111/j.1600-0501.2006.01265.x.
Akkocaoglu, M., Uysal, S., Tekdemir, I., Akca, K., Cehreli, M.C., 2005. Implant design and intraosseous stability of immediately placed implants: a human cadaver study. Clin. Oral Implants Res. 16, 202–209. https://doi.org/10.1111/j.1600-0501.2004.01099.x.
Bay, B.K., Smith, T.S., Fyhrie, D.P., Saad, M., 1999. Digital volume Correlation : three-dimensional strain mapping using X-ray tomography. Exp. Mech. 39, 217–226. https://doi.org/10.1007/bf02323555.
Brunski, J.B., 1992. Biomechanical factors affecting the bone-dental implant interface. Clin. Mater. 10, 153–201. https://doi.org/10.1016/0267-6605(92)90049-Y.
Busse, B., Bale, H. a, Zimmermann, E. a, Panganiban, B., Barth, H.D., Carriero, A., Vettorazzi, E., Zustin, J., Hahn, M., Ager, J.W., Puschel, K., Amling, M., Ritchie, R.O., 2013. Vitamin D deficiency induces early signs of aging in human bone, increasing the risk of fracture. Sci. Transl. Med. 5 https://doi.org/10.1126/scitranslmed.3006286, 193ra88-193ra88.
Cha, J.Y., Pereira, M.D., Smith, a a, Houschyar, K.S., Yin, X., Mouraret, S., Brunski, J.B., Helms, J. a, 2015. Multiscale analyses of the bone-implant interface. J. Dent. Res. 94, 482–490. https://doi.org/10.1177/0022034514566029.
Chen, S.T., Buser, D., 2014. Esthetic outcomes following immediate and early implant placement in the anterior maxilla–a systematic review. Int. J. Oral Maxillofac. Implants 29 (Suppl. l), 186–215. https://doi.org/10.11607/jomi.2014suppl.g3.3.
Chen, S.T., Buser, D., 2009. Clinical and esthetic outcomes of implants placed in postextraction sites. Int. J. Oral Maxillofac. Implants 24 (Suppl. l), 186–217.
Christen, D., Levchuk, A., Schori, S., Schneider, P., Boyd, S.K., Müller, R., 2012. Deformable image registration and 3D strain mapping for the quantitative assessment of cortical bone microdamage. J. Mech. Behav. Biomed. Mater. 8, 184–193. https://doi.org/10.1016/j.jmbbm.2011.12.009.
Chuang, S.F., Chen, T.Y., Chang, C.H., 2008. Application of digital image correlation method to study dental composite shrinkage. Strain 44, 231–238. https://doi.org/10.1111/j.1475-1305.2007.00403.x.
Comini, F., Palanca, M., Cristofolini, L., Dall'Ara, E., 2019. Uncertainties of synchrotron microCT-based digital volume correlation bone strain measurements under simulated deformation. J. Biomech. 86, 232–237. https://doi.org/10.1016/j.jbiomech.2019.01.041.
Cowin, S.C., Hegedus, D.H., 1976. Bone remodeling I: theory of adaptive elasticity. J. Elasticity 6, 313–326. https://doi.org/10.1007/BF00041724.
Dall'Ara, E., Barber, D., Viceconti, M., 2014. About the inevitable compromise between spatial resolution and accuracy of strain measurement for bone tissue: a 3D zero-strain study. J. Biomech. 47, 2956–2963. https://doi.org/10.1016/j.jbiomech.2014.07.019.
de Bakker, C.M.J., Tseng, W.-J., Li, Y., Zhao, H., Altman-Singles, A.R., Jeong, Y., Robberts, J., Han, L., Kim, D.-G., Sherry Liu, X., 2017. Reproduction differentially affects trabecular bone depending on its mechanical versus metabolic role. J. Biomech. Eng. 139, 111006. https://doi.org/10.1115/1.4038110.
Degidi, M., Perrotti, V., Strocchi, R., Piattelli, A., Iezzi, G., 2009. Is insertion torque correlated to bone-implant contact percentage in the early healing period? A histological and histomorphometrical evaluation of 17 human-retrieved dental implants. Clin. Oral Implants Res. 20, 778–781. https://doi.org/10.1111/j.1600-0501.2008.01599.x.
Dorow, C., Krstin, N., Sander, F.-G., 2002. Experiments to determine the material properties of the periodontal ligament. J. Orofac. Orthop./Fortschritte Kieferorthop. 63, 94–104. https://doi.org/10.1007/s00056-002-0107-4.
Du, J., Lee, J.-H., Jang, A.T., Gu, A., Hossaini-Zadeh, M., Prevost, R., Curtis, D.A., Ho, S. P., 2015. Biomechanics and strain mapping in bone as related to immediately-loaded dental implants. J. Biomech. 48, 3486–3494. https://doi.org/10.1016/j.jbiomech.2015.05.014.
French, D., Larjava, H., Ofec, R., 2015. Retrospective cohort study of 4591 Straumann implants in private practice setting, with up to 10-year follow-up. Part 1: multivariate survival analysis. Clin. Oral Implants Res. 26, 1345–1354. https://doi.org/10.1111/clr.12463.
Frost, H.M., 1994. Wolff's Law and Bone's Structural Adaptations to Mechanical Usage: an Overview for Clinicians.
Gallardo, S., Ibañez, M.C., Ibañez, J.C., 2016. Correlation between ISQ and Insertion Torque values using double acid-etched implants. J. Osseointegration 8, 29–36.
Gillard, F., Boardman, R., Mavrogordato, M., Hollis, D., Sinclair, I., Pierron, F., Browne, M., 2014. The application of digital volume correlation (DVC) to study the microstructural behaviour of trabecular bone during compression. J. Mech. Behav. Biomed. Mater. 29, 480–499. https://doi.org/10.1016/j.jmbbm.2013.09.014.
Hammond, M.A., Wallace, J.M., Allen, M.R., Siegmund, T., 2018. Incorporating tissue anisotropy and heterogeneity in finite element models of trabecular bone altered predicted local stress distributions. Biomech. Model. Mechanobiol. 17, 605–614. https://doi.org/10.1007/s10237-017-0981-8.
Hardisty, M.R., Whyne, C.M., 2009. Whole bone strain quantification by image registration: a validation study. J. Biomech. Eng. 131, 064502 https://doi.org/10.1115/1.3127249.
Howell, A.H., Manly, R.S., 1948. An electronic strain gauge for measuring oral forces. J. Dent. Res. 27, 705–712. https://doi.org/10.1177/00220345480270060701.
Hsu, J.-T., Huang, H.-L., Chang, C.-H., Tsai, M.-T., Hung, W.-C., Fuh, L.-J., 2013. Relationship of three-dimensional bone-to-implant contact to primary implant stability and peri-implant bone strain in immediate loading: microcomputed tomographic and in vitro analyses. Int. J. Oral Maxillofac. Implants 28, 367–374. https://doi.org/10.11607/jomi.2407.
Huang, H.-L., Tsai, M.-T., Su, K.-C., Li, Y.-F., Hsu, J.-T., Chang, C.-H., Fuh, L.-J., Wu, A.Y.-J., 2013. Relation between initial implant stability quotient and bone-implant contact percentage: an in vitro model study. Oral Surg. Oral Med. Oral Pathol. Oral Radiol. 116, e356–e361. https://doi.org/10.1016/j.oooo.2012.01.037.
Hussein, A.I., Barbone, P.E., Morgan, E.F., 2012. Digital volume correlation for study of the mechanics of whole bones. Procedia IUTAM 4, 116–125. https://doi.org/10.1016/j.piutam.2012.05.013.
Javed, F., Romanos, G.E., 2010. The role of primary stability for successful immediate loading of dental implants. A literature review. J. Dent. 38, 612–620. https://doi.org/10.1016/j.jdent.2010.05.013.
Jiroušek, O., Jandejsek, I., Vavřík, D., 2011. Evaluation of strain field in microstructures using micro-CT and digital volume correlation. J. Instrum. 6 https://doi.org/10.1088/1748-0221/6/01/C01039. C01039–C01039.
Jun, S., Chang, B.M.W., Weber, H., Kwon, J.-J., 2010. Comparison of initial stability parameters and histomorphometric analysis of implants inserted into extraction sockets: human fresh cadaver study. Int. J. Oral Maxillofac. Implants 25, 985–990.
Kelly, J.R., 1999. Clinically relevant approach to failure testing of all-ceramic restorations. J. Prosthet. Dent 81, 652–661.
Kratochvil, F.J., Caputo, A.A., 1974. Photoelastic analysis of pressure on teeth and bone supporting removable partial dentures. J. Prosthet. Dent 32, 52–61. https://doi.org/10.1016/0022-3913(74)90098-5.
Kusins, J., Knowles, N., Ryan, M., Dall'Ara, E., Ferreira, L., 2019. Performance of QCT-Derived scapula finite element models in predicting local displacements using digital volume correlation. J. Mech. Behav. Biomed. Mater. 97, 339–345. https://doi.org/10.1016/j.jmbbm.2019.05.021.
Launey, M.E., Buehler, M.J., Ritchie, R.O., 2010. On the mechanistic origins of toughness in bone. Annu. Rev. Mater. Res. https://doi.org/10.1146/annurev-matsci-070909-104427.
Le Cann, S., Tudisco, E., Perdikouri, C., Belfrage, O., Kaestner, A., Hall, S., Tägil, M., Isaksson, H., 2017. Characterization of the bone-metal implant interface by Digital Volume Correlation of in-situ loading using neutron tomography. J. Mech. Behav. Biomed. Mater. 75, 271–278. https://doi.org/10.1016/j.jmbbm.2017.07.001.
Leucht, P., Kim, J.B., Wazen, R., Currey, J.A., Nanci, A., Brunski, J.B., Helms, J.A., 2007. Effect of mechanical stimuli on skeletal regeneration around implants. Bone 40, 919–930. https://doi.org/10.1016/j.bone.2006.10.027.
Lioubavina-Hack, N., Lang, N.P., Karring, T., 2006. Significance of primary stability for osseointegration of dental implants. Clin. Oral Implants Res. 17, 244–250. https://doi.org/10.1111/j.1600-0501.2005.01201.x.
Liu, C., Tsai, M.-T., Huang, H.-L., Chen, M.Y.-C., Hsu, J.-T., Su, K.-C., Chang, C.-H., Wu, A.Y.-J., 2012. Relation between insertion torque and bone–implant contact percentage: an artificial bone study. Clin. Oral Invest. 16, 1679–1684. https://doi.org/10.1007/s00784-011-0658-0.
Liu, L., Morgan, E.F., 2007. Accuracy and precision of digital volume correlation in quantifying displacements and strains in trabecular bone. J. Biomech. 40, 3516–3520. https://doi.org/10.1016/j.jbiomech.2007.04.019.
Lloyd, A.A., Gludovatz, B., Riedel, C., Luengo, E.A., Saiyed, R., Marty, E., Lorich, D.G., Lane, J.M., Ritchie, R.O., Busse, B., Donnelly, E., 2017. Atypical fracture with long-term bisphosphonate therapy is associated with altered cortical composition and reduced fracture resistance. Proc. Natl. Acad. Sci. Unit. States Am. 114, 8722–8727. https://doi.org/10.1073/pnas.1704460114.
Manresa, C., Bosch, M., Echeverría, J.J., 2014. The comparison between implant stability quotient and bone-implant contact revisited: an experiment in Beagle dog. Clin. Oral Implants Res. 25, 1213–1221. https://doi.org/10.1111/clr.12256.
Mao, Q., Su, K., Zhou, Y., Hossaini-Zadeh, M., Lewis, G.S., Du, J., 2019. Voxel-based micro-finite element analysis of dental implants in a human cadaveric mandible: tissue modulus assignment and sensitivity analyses. J. Mech. Behav. Biomed. Mater. 94, 229–237. https://doi.org/10.1016/j.jmbbm.2019.03.008.
Nanci, A., Bosshardt, D.D., 2006. Structure of periodontal tissues in health and disease*. Periodontol 40, 11–28. https://doi.org/10.1111/j.1600-0757.2005.00141.x, 2000.
Nanda, R., 2005. Biomechanics and Esthetic Strategies in Clinical Orthodontics, Biomechanics and Esthetic Strategies in Clinical Orthodontics. Elsevier. https://doi.org/10.1016/C2009-0-54720-4.
Oestreich, A.K., Garcia, M.R., Yao, X., Pfeiffer, F.M., Nobakhti, S., Shefelbine, S.J., Wang, Y., Brodeur, A.C., Phillips, C.L., 2015. Characterization of the MPS I-H knock-in mouse reveals increased femoral biomechanical integrity with compromised material strength and altered bone geometry. Mol. Genet. Metab. Reports 5, 3–11. https://doi.org/10.1016/j.ymgmr.2015.08.004.
Park, I.-P., Kim, S.-K., Lee, S.-J., Lee, J.-H., 2011. The relationship between initial implant stability quotient values and bone-to-implant contact ratio in the rabbit tibia. J. Adv. Prosthodont. 3, 76. https://doi.org/10.4047/jap.2011.3.2.76.
Perosky, J.E., Khoury, B.M., Jenks, T.N., Ward, F.S., Cortright, K., Meyer, B., Barton, D. K., Sinder, B.P., Marini, J.C., Caird, M.S., Kozloff, K.M., 2016. Single dose of bisphosphonate preserves gains in bone mass following cessation of sclerostin antibody in Brtl/+ osteogenesis imperfecta model. Bone 93, 79–85. https://doi.org/10.1016/j.bone.2016.09.013.
Proff, P., Bayerlein, T., Rottner, K., Mai, R., Fanghänel, J., Gedrange, T., 2008. Effect of bone conditioning on primary stability of FRIALIT-2 ® implants. Clin. Oral Implants Res. https://doi.org/10.1111/j.1600-0501.2007.01400.x.
Rho, J.Y., Kuhn-Spearing, L., Zioupos, P., 1998. Mechanical properties and the hierarchical structure of bone. Med. Eng. Phys. 20, 92–102. https://doi.org/10.1016/S1350-4533(98)00007-1.
Ritchie, R.O., Buehler, M.J., Hansma, P., 2009. Plasticity and toughness in bone. Phys. Today 62, 41–47. https://doi.org/10.1063/1.3156332.
Roberts, W.E., Huja, S., Roberts, J.A., 2004. Bone modeling: biomechanics, molecular mechanisms, and clinical perspectives. Semin. Orthod. 10, 123–161. https://doi.org/10.1053/j.sodo.2004.01.003.
Scarano, A., Degidi, M., Iezzi, G., Petrone, G., Piattelli, A., 2006. Correlation between implant stability quotient and bone-implant contact: a retrospective histological and

histomorphometrical study of seven titanium implants retrieved from humans. Clin. Implant Dent. Relat. Res. 8, 218–222. https://doi.org/10.1111/j.1708-8208.2006.00022.x.

Scheller, E.L., Khoury, B., Moller, K.L., Wee, N.K.Y., Khandaker, S., Kozloff, K.M., Abrishami, S.H., Zamarron, B.F., Singer, K., 2016. Changes in skeletal integrity and marrow adiposity during high-fat diet and after weight loss. Front. Endocrinol. 7, 102. https://doi.org/10.3389/fendo.2016.00102.

Schlegel, A.K., Donath, K., 1998. BIO-OSS–a resorbable bone substitute? J. Long Term Eff. Med. Implants 8, 201–209.

Tozzi, G., Danesi, V., Palanca, M., Cristofolini, L., 2016. Elastic full-field strain analysis and microdamage progression in the vertebral body from digital volume correlation. Strain 52, 446–455. https://doi.org/10.1111/str.12202.

Tozzi, G., Zhang, Q.-H., Tong, J., 2012. 3D real-time micromechanical compressive behaviour of bone–cement interface: experimental and finite element studies. J. Biomech. 45, 356–363. https://doi.org/10.1016/j.jbiomech.2011.10.011.

Turkyilmaz, I., Sennerby, L., McGlumphy, E.A., Tözüm, T.F., 2009. Biomechanical aspects of primary implant stability: a human cadaver study. Clin. Implant Dent. Relat. Res. 11, 113–119. https://doi.org/10.1111/j.1708-8208.2008.00097.x.

Veis, A.A., Papadimitriou, S., Trisi, P., Tsirlis, A.T., Parissis, N.A., Kenealy, J.N., 2007. Osseointegration of Osseotite and machined-surfaced titanium implants in membrane-covered critical-sized defects: a histologic and histometric study in dogs. Clin. Oral Implants Res. 18, 153–160. https://doi.org/10.1111/j.1600-0501.2006.01316.x.

Verhulp, E., Rietbergen, B. Van, Huiskes, R., 2004. A three-dimensional digital image correlation technique for strain measurements in microstructures. Exp. Mech. 37, 1313–1320. https://doi.org/10.1016/j.jbiomech.2003.12.036.

Verner, K.A., Lehner, M., Lamas, L.P., Main, R.P., 2016. Experimental tests of planar strain theory for predicting bone cross-sectional longitudinal and shear strains. J. Exp. Biol. https://doi.org/10.1242/jeb.134536.

Wang, R.Z., Weiner, S., 1998. Strain-structure relations in human teeth using Moiré fringes. J. Biomech. 31, 135–141.

Wazen, R.M., Currey, J.A., Guo, H., Brunski, J.B., Helms, J.A., Nanci, A., 2013. Micromotion-induced strain fields influence early stages of repair at bone-implant interfaces. Acta Biomater. 9, 6663–6674. https://doi.org/10.1016/j.actbio.2013.01.014.

Wolff, J., 1986. The law of bone remodelling, the law of bone remodelling. https://doi.org/10.1007/978-3-642-71031-5.

Yang, H., Embry, R.E., Main, R.P., 2017. Effects of loading duration and short rest insertion on cancellous and cortical bone adaptation in the mouse tibia. PloS One. https://doi.org/10.1371/journal.pone.0169519.

Yoda, N., Zheng, K., Chen, J., Li, W., Swain, M., Sasaki, K., Li, Q., 2017. Bone morphological effects on post-implantation remodeling of maxillary anterior buccal bone: a clinical and biomechanical study. J. Prosthodont. Res. 61, 393–402. https://doi.org/10.1016/j.jpor.2016.12.010.

Yoshida, N., Koga, Y., Peng, C.-L., Tanaka, E., Kobayashi, K., 2001. In vivo measurement of the elastic modulus of the human periodontal ligament. Med. Eng. Phys. 23, 567–572. https://doi.org/10.1016/S1350-4533(01)00073-X.

Zauel, R., Yeni, Y.N., Bay, B.K., Dong, X.N., Fyhrie, D.P., 2006. Comparison of the linear finite element prediction of deformation and strain of human cancellous bone to 3D digital volume correlation measurements. J. Biomech. Eng. 128, 1–6. https://doi.org/10.1115/1.2146001.

Zhang, D., Arola, D.D., Rouland, J.A., 2001. Evaluating the elastic modulus of bone using electronic speckle pattern interferometry. Exp. Tech. 25, 32–34. https://doi.org/10.1111/j.1747-1567.2001.tb00039.x.

Zhang, Y.-R., Du, W., Zhou, X.-D., Yu, H.-Y., 2014. Review of research on the mechanical properties of the human tooth. Int. J. Oral Sci. 6, 61–69. https://doi.org/10.1038/ijos.2014.21.

Zhou, Y., Gong, C., Lewis, G.S., Armstrong, A.D., Du, J., 2019. 3D full-field biomechanical testing of a glenoid before and after implant placement. Extrem. Mech. Lett. 100614 https://doi.org/10.1016/j.eml.2019.100614.

Zhu, M.L., Zhang, Q.H., Lupton, C., Tong, J., 2016. Spatial resolution and measurement uncertainty of strains in bone and bone-cement interface using digital volume correlation. J. Mech. Behav. Biomed. Mater. 57, 269–279. https://doi.org/10.1016/j.jmbbm.2015.12.017.

Zimmermann, E.A., Ritchie, R.O., 2015. Bone as a structural material. Adv. Healthc. Mater. 4, 1287–1304. https://doi.org/10.1002/adhm.201500070.

Zimmermann, E.A., Schaible, E., Bale, H., Barth, H.D., Tang, S.Y., Reichert, P., Busse, B., Alliston, T., Ager, J.W., Ritchie, R.O., 2011. Age-related changes in the plasticity and toughness of human cortical bone at multiple length scales. Proc. Natl. Acad. Sci. Unit. States Am. 108, 14416–14421. https://doi.org/10.1073/pnas.1107966108.